Raytheon
Customer Success Is Our Mission

Polarimetric Observations of Prescribed Bushfires in South Australia using a Phased Array Radar

Robert Palumbo, Waddah A. Al-Ashwal, Stephen J. Frasier, Bradley Ferguson, David J. McLaughlin, Eric J. Knapp, Christopher McCarroll,

AMS 36th Conference on Radar Meteorology
19 September 2013

Acknowledge
Douglas Gray
University of Adelaide, Adelaide, SA, AU
P. Keith Kelly
First RF Corporation, Boulder, CO, USA
Mike Wouters
Department of Environment, Water and Natural Resources (DEWNR), SA, AU

FIRST RF Corporation
Raytheon
THE UNIVERSITY of ADELAIDE
UMASS AMHERST
National Science Foundation
WHERE DISCOVERIES BEGIN

Problem Statement
Wildfires as a Global Threat

- Wildfires are persistent threat across the globe
  - Recent fires in Arizona, US killed 19 firefighters, “outflanked by wind-whipped flames in seconds” [1]
- Firefighters on the frontline need a faster method for monitoring bushfire spread and environmental conditions
- Microwave sensors offer the capability for bushfire observation, but more research needs to be done to characterize the scattering properties of smoke plume returns

A firefighter observes a wildfire near Lake Hughes, CA, US [2]

A bushfire rages in Cherryville, SA, AU

There is a need for a faster and more accurate method of bushfire detection and monitoring

Radar System Parameters
Specifications

Parameter	Units	
Center Frequency	GHz	9.41
Transmit Power (Peak)	W	70
Pulse Length	µS	.6 - 40
Pulse Compression Gain	dB	Up to 20
Duty Cycle (max)		30%
Unambiguous range @ max PRF	km	31
Unambiguous Velocity @ single PRF	m/s	up to 38
Unambiguous Velocity @ Dual PRF	m/s	57 @ (2:3)
Sensitivity @ 35km	dBZ	12
Elevation Beamwidth	deg	2.8
Azimuth Beamwidth	deg	1.8 -2.4
Polarization Mode		Alternating
Integrated Cross Pol Ratio (max)	dB	-20
Power Consumption		600W (average)

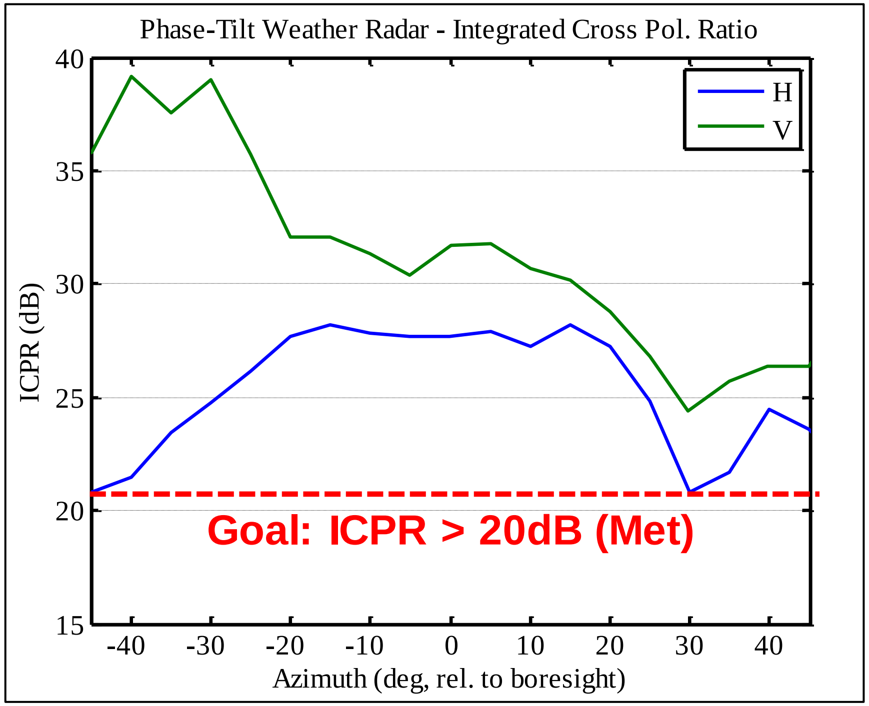

Test Methodology
Overview

- Nine bushfires observed over 5-week period
  - Mostly prescribed burns in Adelaide Hills region
  - Observed uncontrolled Cherryville Bushfire (09/10-May)

- Assumptions:
  - Plume returns as volumetric target (randomly distributed scatterers within volume)
  - Plume returns are incoherent [11]
  - Uniform beam-filling: due to small angular resolution (100m x 84m @ 2km)

Burn Site	Date	Area Burned (ha) (acres)	Ignition
Belair CP	4-April-2013	9.0 (22.2)	strip head
	5-April-2013	16.9 (41.8)	strip head
South Para Reservoir	10-April-2013	26.0 (64.2)	strip head
Barossa Reservoir	17-April-2013	47.6 (117.6)	aerial
Cleland CP	28-April-2013	10.0 (24.7)	strip head
Cox Scrub CP	1-May-2013	40.0 (98.8)	strip head
Kyeema CP	2-May-2013	39.6 (97.8)	strip head
Cherryville	9-May-2013	650 (1600)	uncontrolled
	10-May-2013	650 (1600)	uncontrolled

Observed bushfire dates and locations, showing burn area and ignition type.

Observations
Scattering Mechanism

- During prescribed burn on 4 April 2013, collected data samples from fallen ash
- Predominantly two types of ash particles observed
  - Plate-like leaf ash (5cm – 15cm, <1cm thick)
  - Spheroidal or ellipsoidal masses from burnt grass and scrub (axial radii 5cm – 15cm)
- Observations correlate with previous work
  - Banta et al. (1992) used Circular Depolarization Ratio measurements to identify particles as having “flat, needle-like” shape
  - Melnikov et al. (2009) modeled debris shape as spheroidal with unknown rotation angle
- Results show large debris particle sizes, which may indicate Mie scattering is occurring within the smoke plume at X-band
  - Result is inconclusive until further research is done into the distribution of shapes at microwave wavelengths

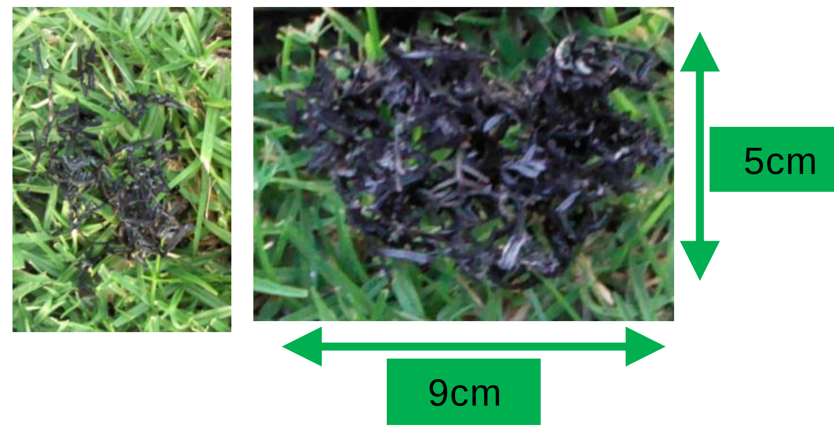

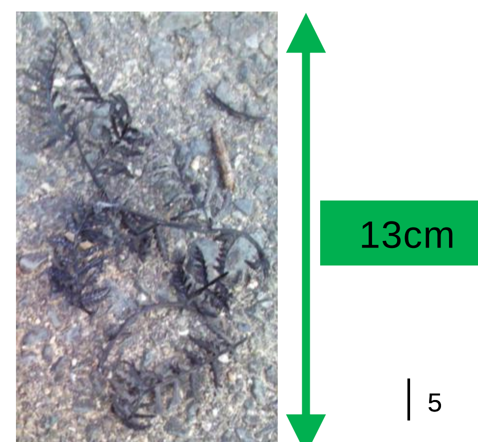

Observations

- Following slides show observations from two bushfires:
  - Prescribed burn at Barossa Valley Reservoir (17 April 2013)
    - Ignited via aerial methods (helicopter with ignited petroleum jelly)
    - Aerial-ignited burns create more intense fires than standard strip burning methods
  - Uncontrolled bushfire near Cherryville, SA (10 May 2013)
    - Over course of four days, uncontrolled bushfire destroyed over 650Ha of urban land in regions north of Adelaide, SA

Observations

Prescribed Burn (17 April 2013)

- Following slides show Range-Height Indicator (RHI) scans taken at peak intensity during the prescribed burn
- Observations:
  - Reflectivity appears to be higher in areas above the (assumed) active fire source, compared with the photography
  - Storm-relative velocity shows chaotic and turbulent mixing occurring within the smoke plume

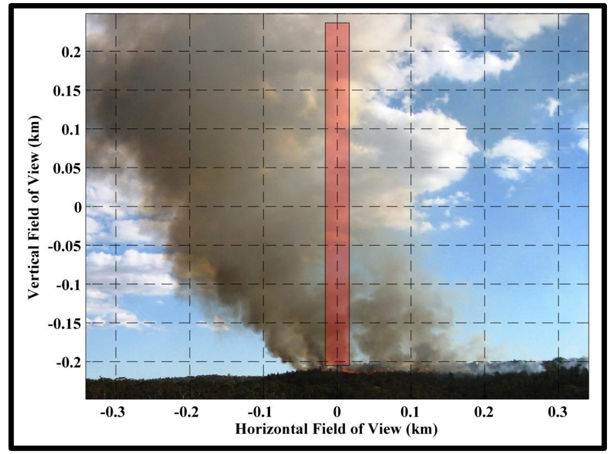

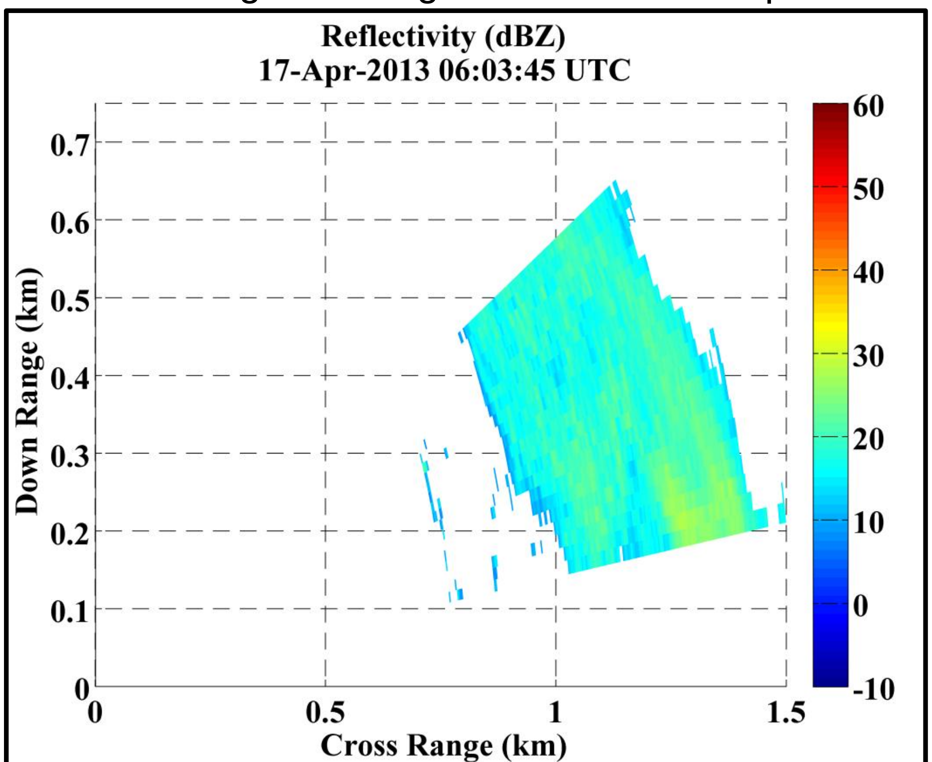

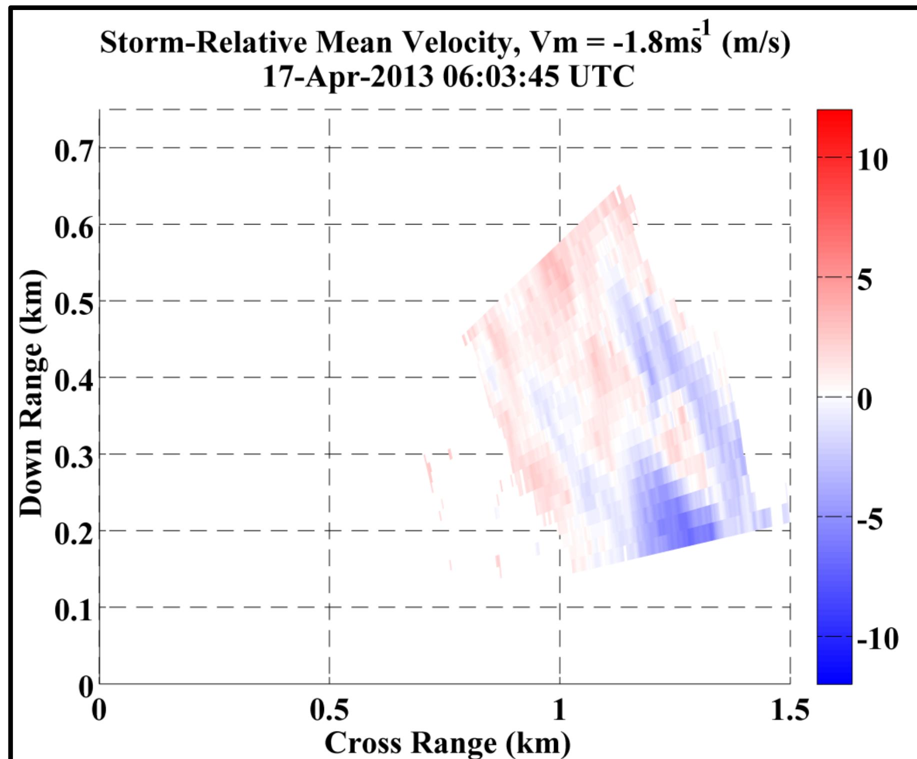

Observations
Prescribed Burn: Differential Reflectivity

- RHI scans performed during prescribed burn show localized increases in Z_{DR} within the plume
- Observations:
  - Reduced mean Z_{DR} above fire sources
    - Luchs et al (2013) have made the same observation [15]
  - Higher Z_{DR} with higher extremes and "spikes" away from the fire source

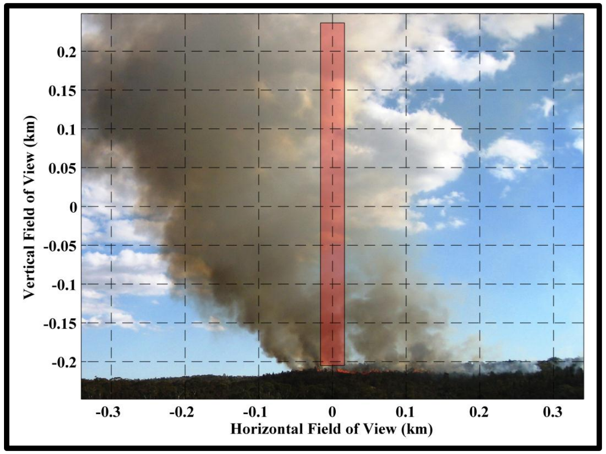

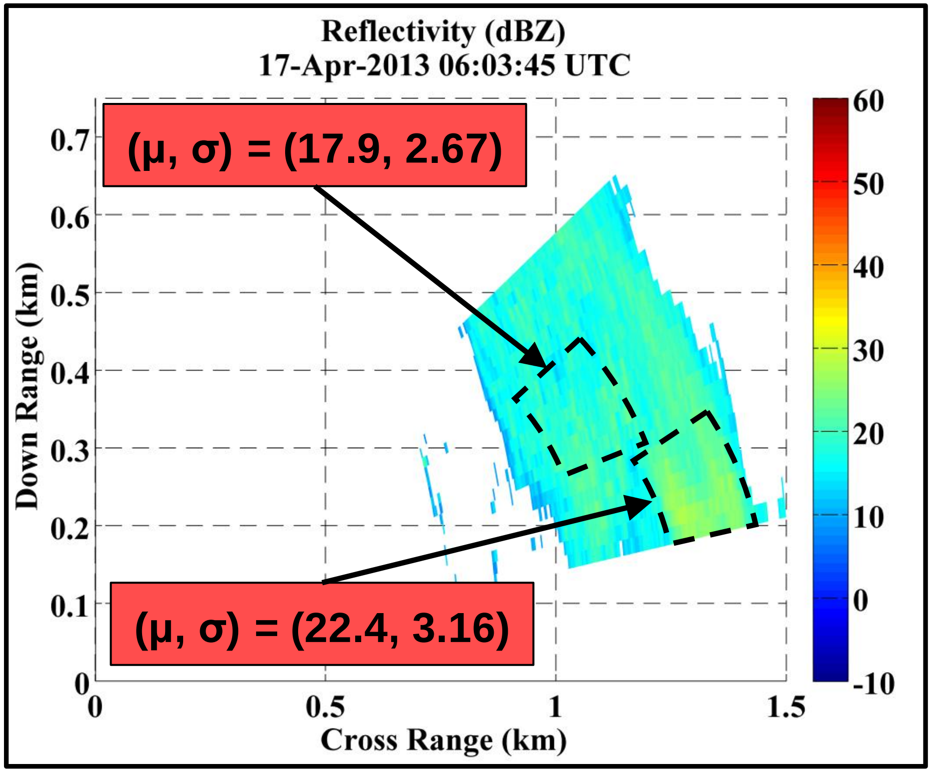

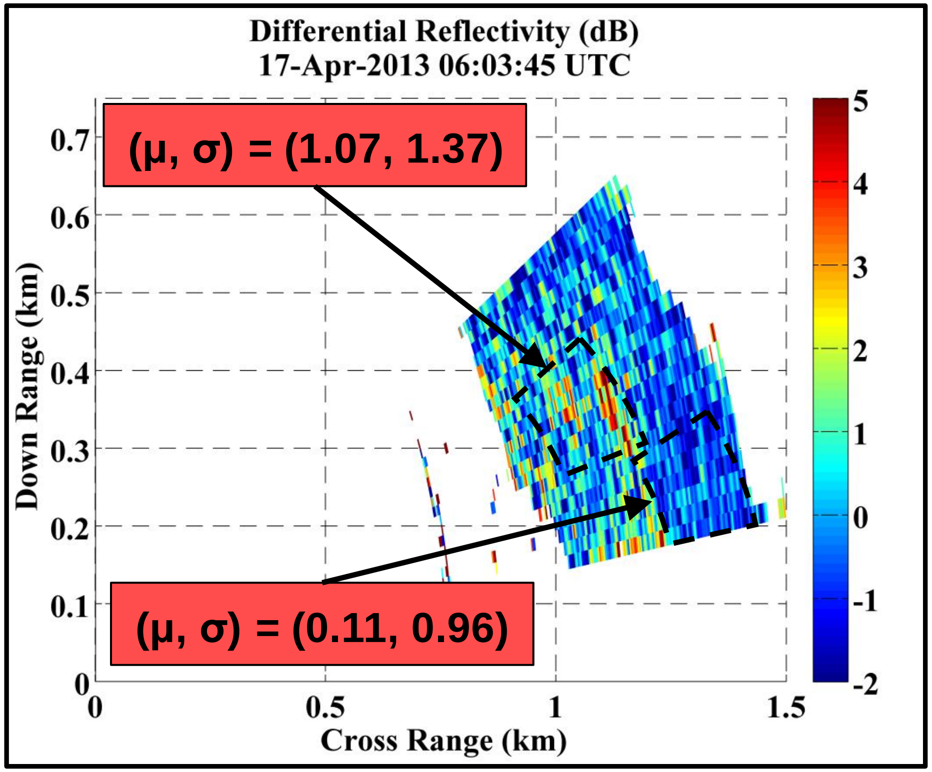

Observations

Prescribed Burn: Copolar Correlation Coefficient

- At the same timestamp, ρ_{hv} shows no definitive pattern compared to reflectivity or other measurements
- Some variation in ρ_{hv} likely due to statistical fluctuations within the smoke plume
  – Studies and field work have suggested that condensed water vapor or mist can be created during intense fires [16], which could lead to higher values of ρ_{hv} (> 0.9)
  – No conclusive evidence of high ρ_{hv} leads to the conclusion that either water vapor not formed during fires or the mixing of water droplets and debris particles would still cause lower values

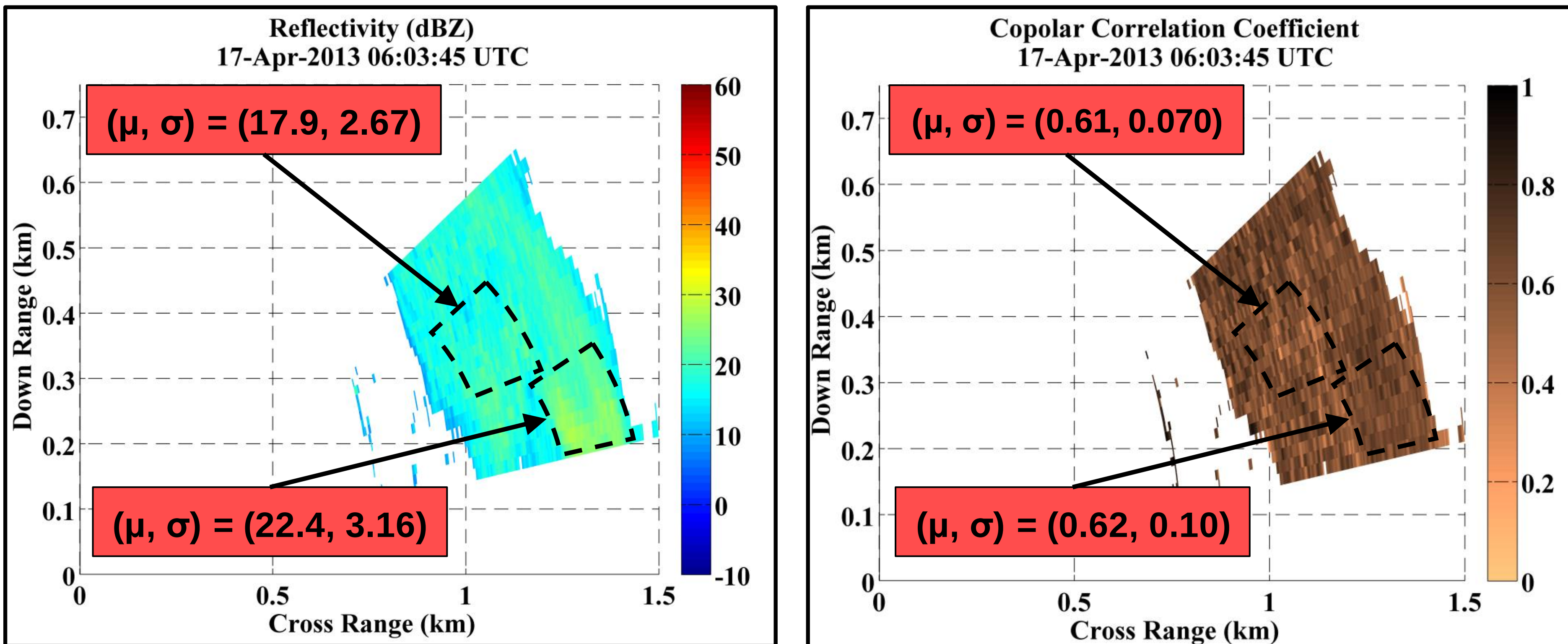

Observations

Prescribed Burn: Differential Phase

- Data shows high local variation of differential phase, between 10° and 20° per 50m range span
  - Indicative of high backscatter differential phase, as opposed to precipitation having low backscatter differential phase
  - Observation agrees with previous work [7]
- Similar to Z_{DR}, reduced mean and variation above fire sources

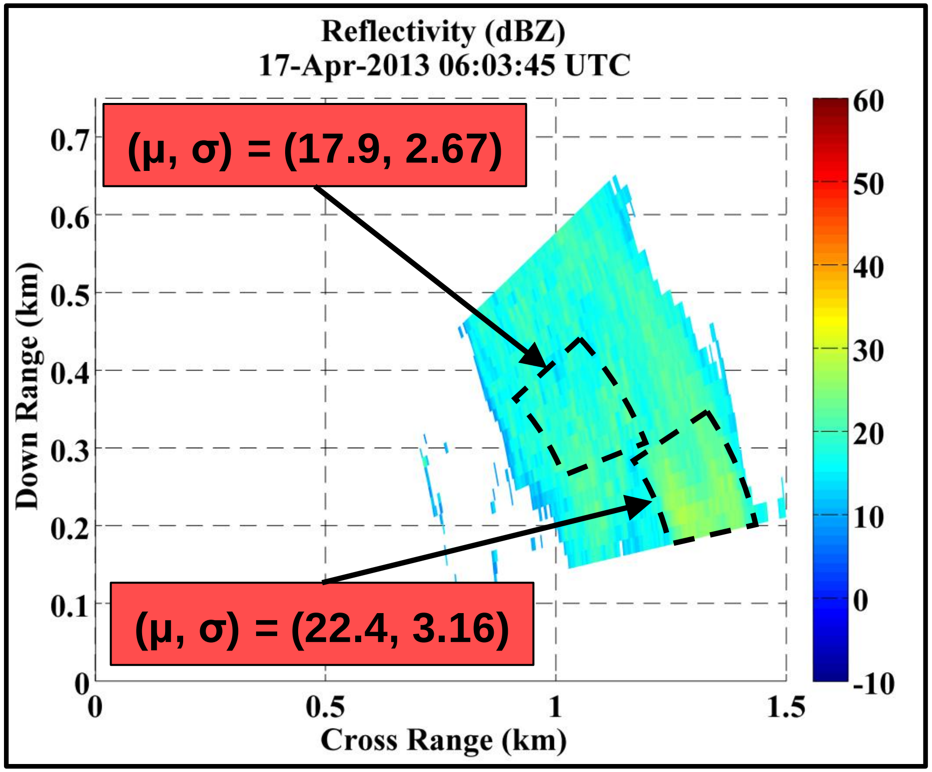

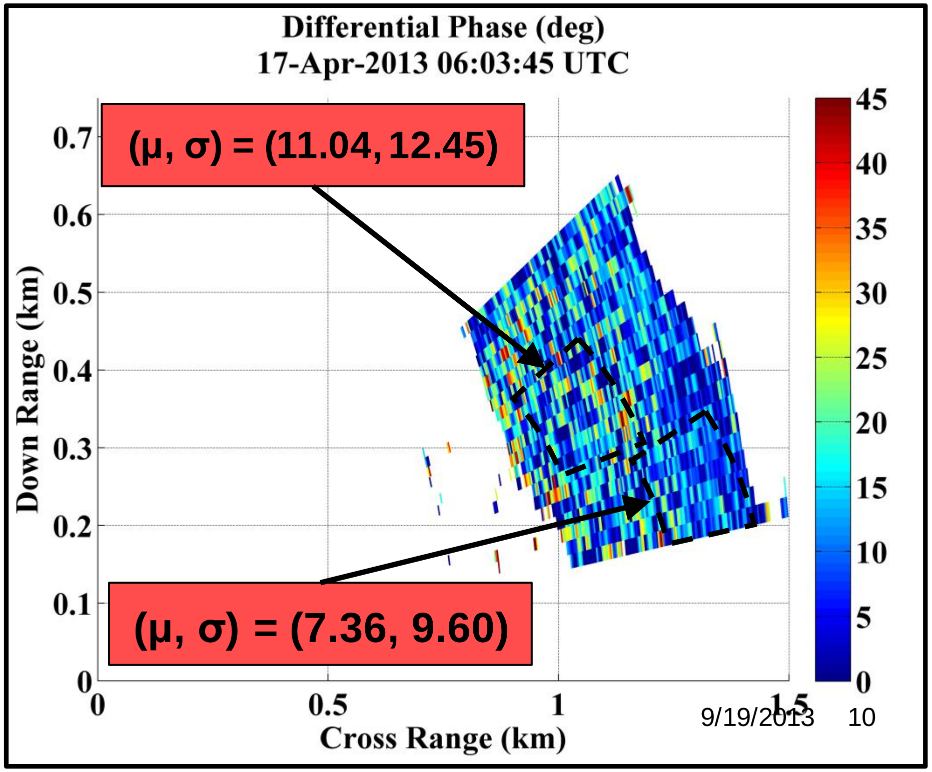

Observations

Uncontrolled Bushfire: Differential Reflectivity

- Azimuth Planned Position Indicator (PPI) scans during an uncontrolled bushfire show the same Z_{DR} pattern
  - Reduced mean and variation of ZDR in areas with higher reflectivity
- As before, active fire sources are indicated as regions with higher reflectivity
  - Plume orientation aligns with local ground wind direction

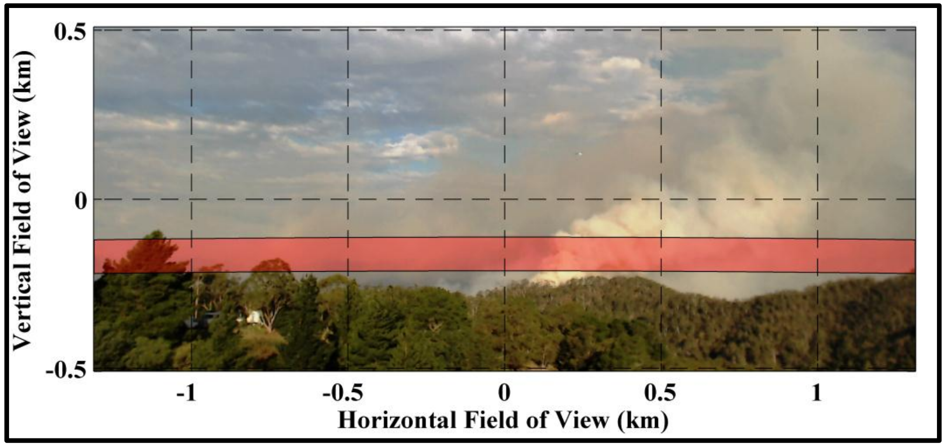

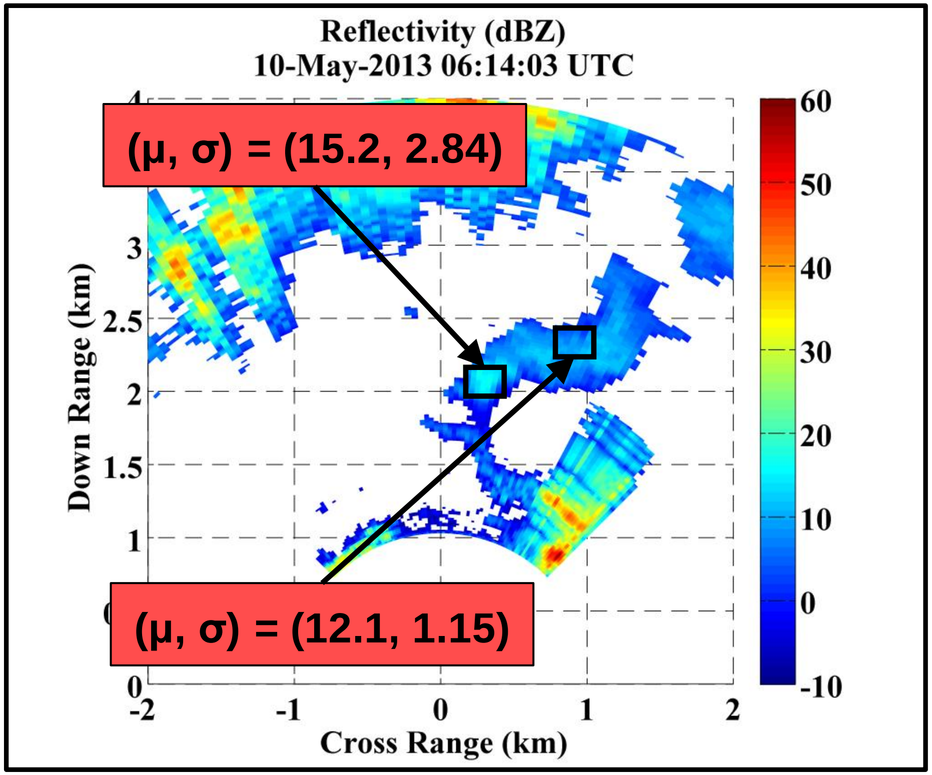

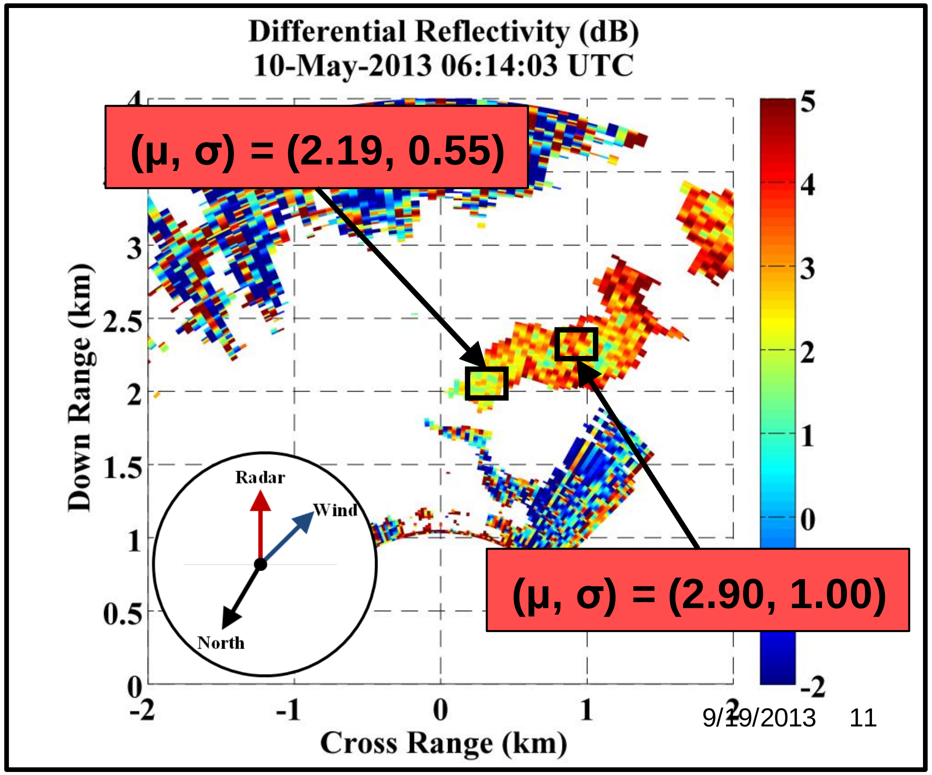

Discussion

Smoke Plume Model Hypothesis

- From the observations and analysis made, propose the following model to describe the scattering mechanism within the smoke plume:
  - **Above the fire source**:
    - Larger particles tumble more quickly about their axis as they are propelled upwards
      - Tumbling particles appear to have a lower differential reflectivity because they scatter more in each polarization
  - **Away and downwind from the fire source**:
    - Larger particles fall to the ground while smaller, lighter particles tend to float or drift with their major axis parallel to the ground
      - Predominantly ellipsoidal-shaped particles (i.e. leaf matter) drifting in the wind produces a reduced differential reflectivity

Conclusion

- X-band polarimetric observations presented from prescribed burns and uncontrolled bushfires in South Australia

- Observations:
  - Increased reflectivity above the active fire source
  - Positive differential reflectivity everywhere
    - Reduced mean and variation above fire source, higher in areas downwind
  - Low copolar correlation coefficient (0.4 – 0.7)
  - Large backscatter differential phase through the smoke plume, 10° - 20°

- From observations, proposed a hypothesis to explain polarimetric signature:
  - "Two scattering mechanism model": Tumbling debris above fire source in convection column versus downwind drifting particles

Questions?

Bibliography (1)

- [1] Gaynor, Tim. “Deadly fire engulfed 19 Arizona firefighters in seconds”. Reuters, Jul. 2013. Available: http://www.reuters.com/article/2013/07/01/us-usa-fires-arizona-idUSBRE96003520130701
- [2] Diana Soliwon, “Photos: Arizona Firefighter Deaths Mark Active Wildfire Season” (US News and World Report, Jul. 2013), Available: http://www.usnews.com/news/articles/2013/07/01/photos-arizona-firefighter-deaths-mark-active-wildfire-season.
- [3] Cheal, David. *Growth stages and tolerable fire intervals for Victoria’s native vegetation data sets*. vols. Fire and Adaptive Management Report No. 84. The Victorian Government Department of Sustainability and Environment Melbourne, 2010.
- [4] Stuart Ellis, Peter Kanowski, and RJ Whelan, “National inquiry on bushfire mitigation and management” (2004).
- [5] Banta, RM et al. “Smoke-column observations from two forest fires using Doppler lidar and Doppler radar.” *Journal of Applied Meteorology* 31.11 (1992): 1328–1349.
- [6] T.A. Jones and S.A. Christopher, “Satellite and radar remote sensing of Southern Plains grass fires: a case study,” *Journal of Applied Meteorology and Climatology* 49 (2010): 2133–2146.
- [7] V Melnikov et al., “Radar polarimetric signatures of fire plumes,” in *Proc. 25th Conference on International Interactive Information and Processing Systems*, vols., 2009.
- [8] P.S. Tsai et al., “Combined LiDAR and radar observations of smoke plumes from prescribed burns,” in *Proc. The Fourth Symposium on LiDAR Atmospheric Applications*, vols., 2009, 10–16.
- [9] Kamran Ghorbani, Thomas C Baum, and Lachlan Thompson, “Properties and Radar Cross-Section of forest fire ash particles at millimeter wave,” in *The 42nd European Microwave Conference (EuMC’12)*, vols., 2012, 1335–1338
- [10] T. Baum, L. Thompson, and K. Ghorbani, “A Complex Dielectric Mixing Law Model for Forest Fire Ash Particulates,” *IEEE_J_GRSL* 9 (2012): 832–835.
- [11] JS Erkelens et al., “Coherent scattering of microwaves by particles: Evidence from clouds and smoke,” *Journal of the atmospheric sciences* 58 (2001): 1091–1102.

Bibliography (2)

- [12] R.J. Doviak and D.S. Zrnic, *Doppler Radar And Weather Observations*, vols. (Dover Publications, 1993).
- [13] V.N. Bringi and V. Chandrasekar, *Polarimetric Doppler Weather Radar: Principles and Applications*, vols. (Cambridge University Press, 2001).
- [14] Thomas Meissner and Frank J Wentz, “The complex dielectric constant of pure and sea water from microwave satellite observations,” *Geoscience and Remote Sensing, IEEE Transactions on* 42 (2004): 1836–1849.
- [15] S Luchs and J Pendergrast, “Using Dual Polarimetric Radar to Assess Prescribed and Wildland Fire Intensity in Florida,” in *Proc. 17th Conference on Integrated Observing and Assimilation Systems for the Atmosphere, Oceans, and Land Surface (IOAS-AOLS’13)*, vols. (American Meteorological Society, 2013).
- [16] Lawrence F Radke et al., “Particulate and trace gas emissions from large biomass fires in North America,” *Global Biomass Burning: Atmospheric Climatic and Biospheric Implications* (1991).

Backup

System Overview
Main Components

- Three main subsystems:

Array Subsystem
Self-contained outdoor phase-tilt antenna array subsystem (First RF©)

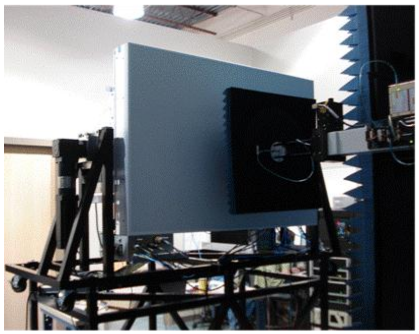

Digital IF Transceiver
COTs adapted

PC Processor
Host PC runs signal processing, scan commands and display

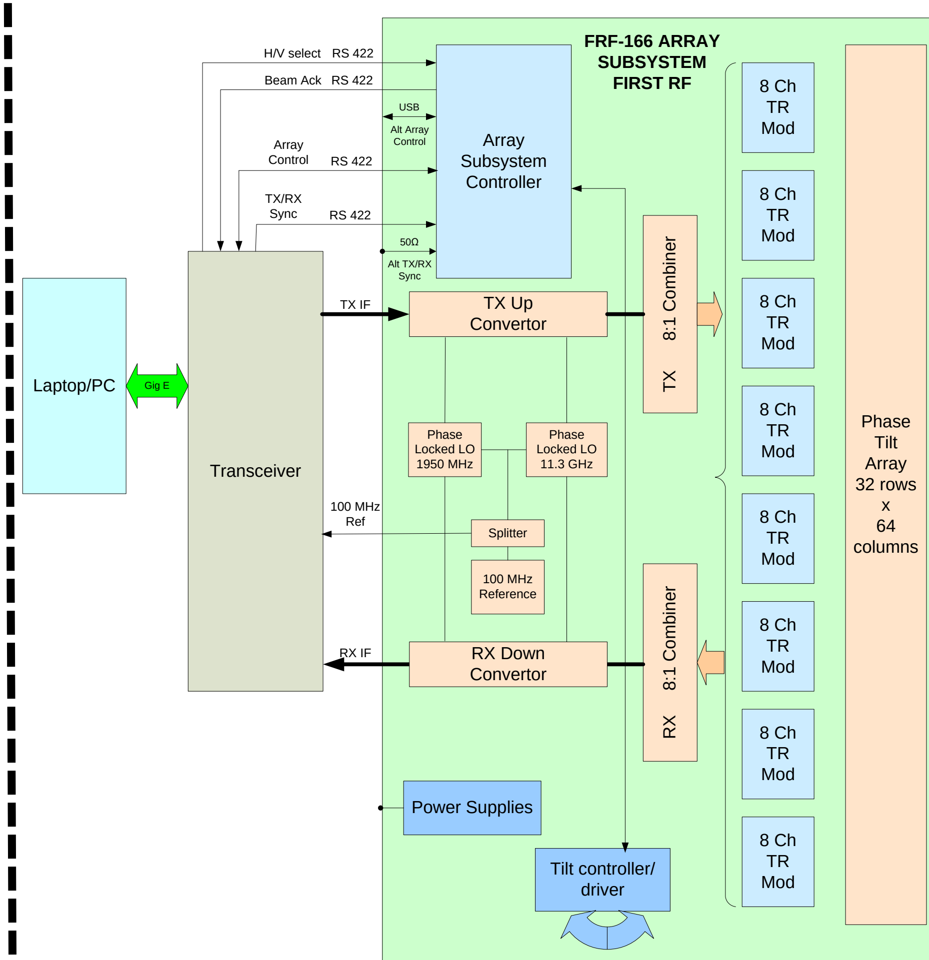

Test Methodology

Radar Waveforms

- To optimize sensitivity and range resolution, used four different waveforms at each burn with different range resolutions:
  - 1-5μs, CW Pulse
  - 1-5μs, 3MHz LFM (50m range resolution)
  - 1-5μs, 10MHz LFM (15m range resolution)
  - 1-5μs, 23MHz LFM (7m range resolution)

- Sensitivity curves below show trade-off of minimum sensitivity as waveform range resolution is varied

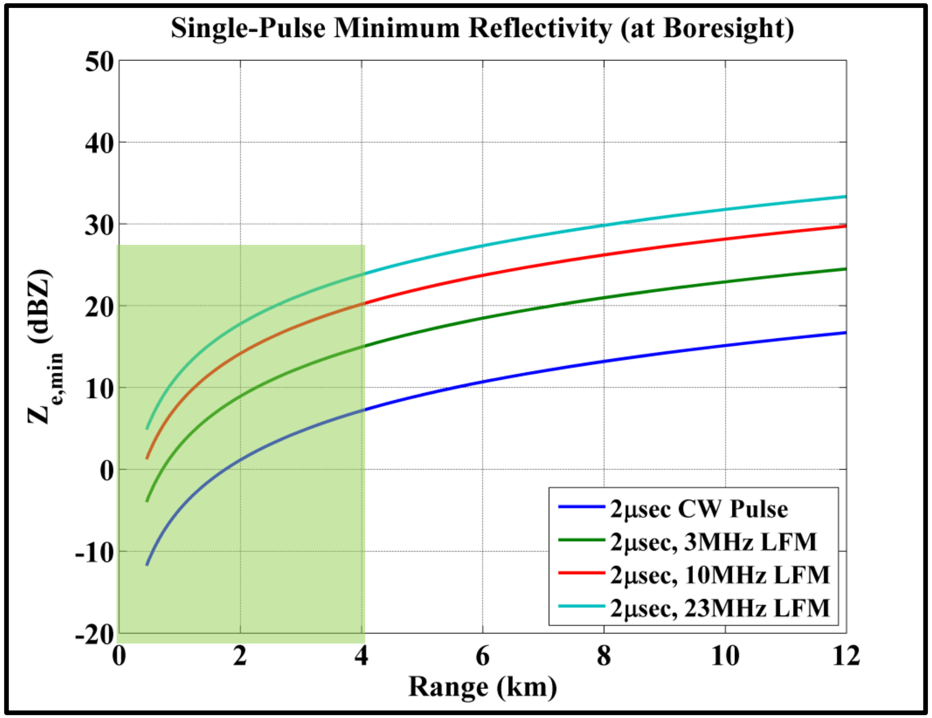

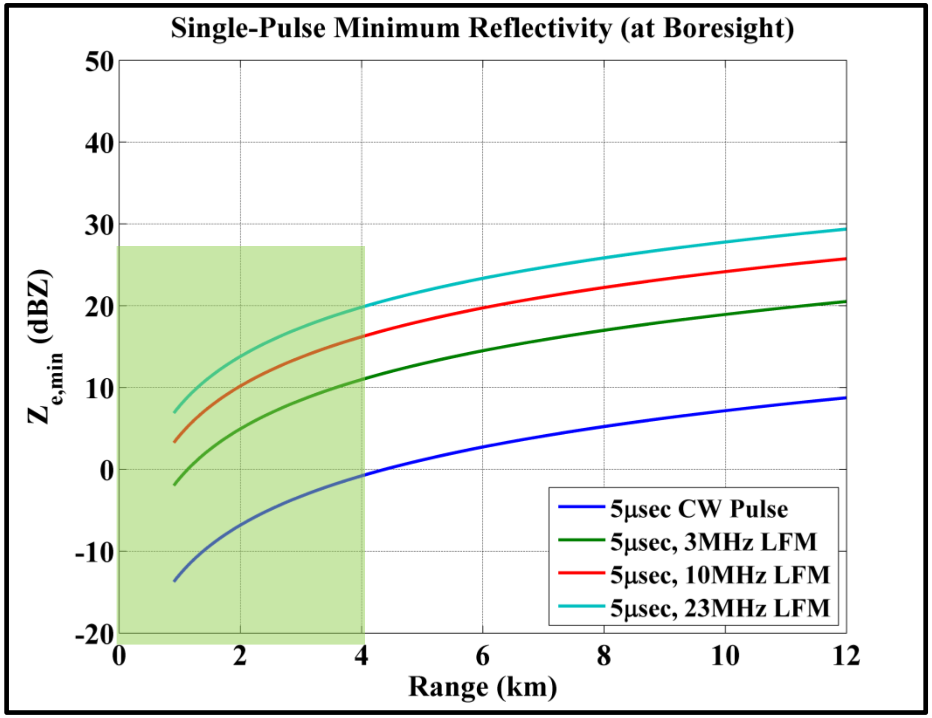

Observations

Scattering Mechanism

- Two species of Australian flora were identified from the ash debris collected: Bracken Fern and Gum Tree

- Table below shows the complex dielectric constant and dielectric factor of common species in Australia
  - Lower dielectric constant compared to that of water indicates low moisture content
  - This data shows that bushfire plume returns will have a lower measured reflectivity than that of precipitation[1], assuming equivalent volumetric contents

Species	ε_i	$tan(\delta)$	$\rho(g/cc)$	K_w
Water	$63.39 + 28.76j$	0.4537	≈ 1.0	0.93
Eucalypt	$6.30 + 0.06j$	0.0095	2.84	0.41
Bracken Fern	$4.85 + 0.51j$	0.2052	1.95	0.32
. She Oak	$10.05 + 2.76j$	0.1751	2.95	0.59
Wattle Tree	$11.44 + 1.71j$	0.1495	2.01	0.61
Cypress	$8.68 + 0.85j$	0.0979	2.35	0.52
Pine	$16.99 + 3.51j$	0.1854	2.11	0.72

Measured dielectric constants and dielectric factors of Australian flora at X-band (10GHz), compared to that of water at room temperature (Meissner and Wentz 2004; Baum et al. 2012) [14,10]

[1]Reflection coefficient is proportional to dielectric constant of the scattering medium, so a lower dielectric constant reduces the backscattered energy

Test Methodology
Derivation of Copolar Correlation Coefficient Estimate

- From [13]:

Assuming Gaussian Doppler spectrum, have

$$|\rho^n| = e^{-8\pi^2\sigma_v^2 n^2 T_s^2/\lambda^2}$$

So, we can write $|\rho[1]|$ in terms of $|\rho[2]|$ as

$$|\rho^1| = |\rho^2|^{(1/2)^2} = |\rho^2|^{1/4}$$

And, combined with an approximation by Sachidananda and Zyrnć (1985)

$$\hat{\rho}_{hv}^1 = \hat{\rho}_{hv}^0 \hat{\rho}_{hh}^1$$

Since we don’t have $\hat{\rho}_{hh}^1$, we need to estimate it from $\hat{\rho}_{hh}^2$, so we have

$$\hat{\rho}_{hv}^0 = \frac{\hat{\rho}_{hv}^1}{\left|\hat{\rho}_{hh}^2\right|^{0.25}}$$

From which we arrive at our lag-0 estimate of the copolar correlation coefficient

Test Methodology
Derivation of Differential Phase

- From [13]:

Start with an approximation by Sachidananda and Zyrnć (1985)

$$\hat{\rho}_{hv}^{1} = \hat{\rho}_{hv}^{0}\hat{\rho}_{hh}^{1}$$
$$\hat{\rho}_{vh}^{1} = \hat{\rho}_{vh}^{0}\hat{\rho}_{vv}^{1}$$

Taking the argument for each one above to compute the phase, we have

$$\arg\left[\hat{\rho}_{hv}^{1}\right] = \arg\hat{\rho}_{hv}^{0}\hat{\rho}_{hh}^{1} = \varphi_{DP} + \arg[\hat{\rho}_{hh}^{1}]$$
$$\arg\left[\hat{\rho}_{vh}^{1}\right] = \arg\hat{\rho}_{vh}^{0}\hat{\rho}_{vv}^{1} = -\varphi_{DP} + \arg[\hat{\rho}_{vv}^{1}]$$

Since φ_{DP} is defined as $\arg\hat{\rho}_{hv}^{0}$ and, by reciprocity, $\hat{R}_{hh,vv}^{1} = \left(\hat{R}_{vv,hh}^{1}\right)^{*}$.

From this, we see how we get φ_{DP} from the arguments of the lag-1 copolar correlation coefficients. Here, they make the assumption that $\hat{\rho}_{hh}^{1}$=$\hat{\rho}_{vv}^{1}$.

Observations
Waveform Trade Study (1)

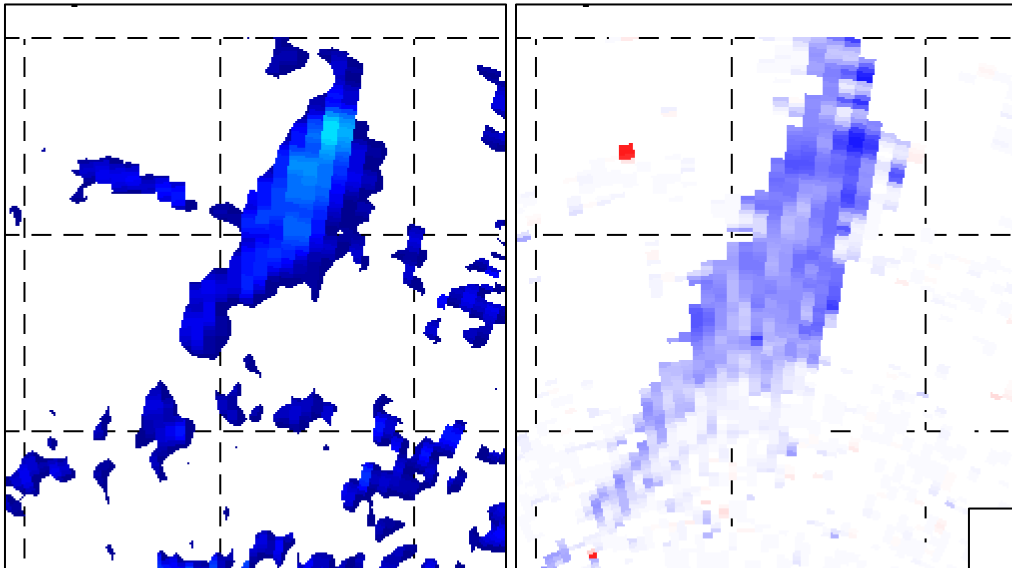

Reflectivity
01-May-2013 06:57:20 UTC

Radial Velocity
01-May-2013 06:57:20 UTC

5µsec 3MHz LFM Waveform
(50m range resolution)

5µsec 10MHz LFM Waveform
(15m range resolution)

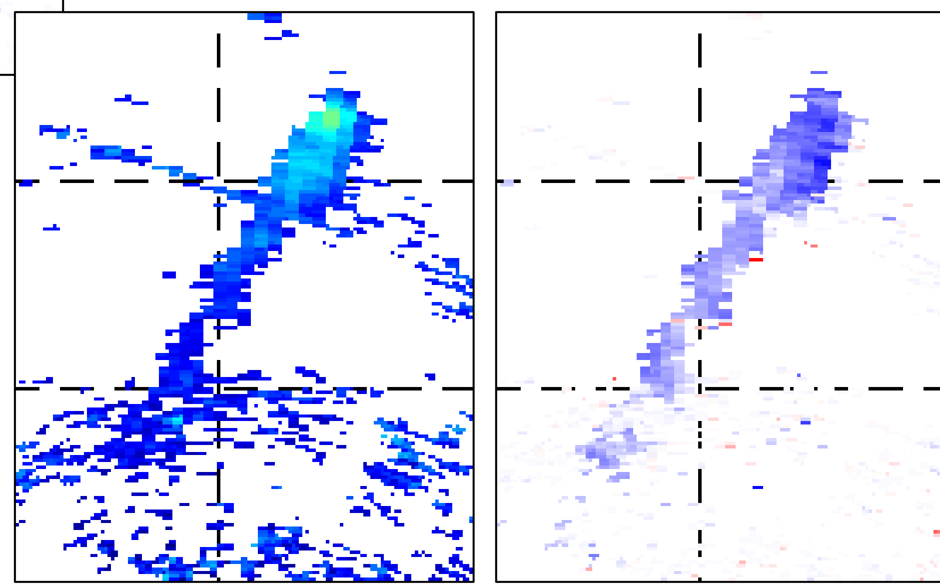

Reflectivity (dBZ)
01-May-2013 06:57:46 UTC

Radial Velocity (m/s)
01-May-2013 06:57:46 UTC

Observations
Waveform Trade Study (2)

- Waveform trade study during Cherryville bushfire
  - Datasets within 5 minutes of each other

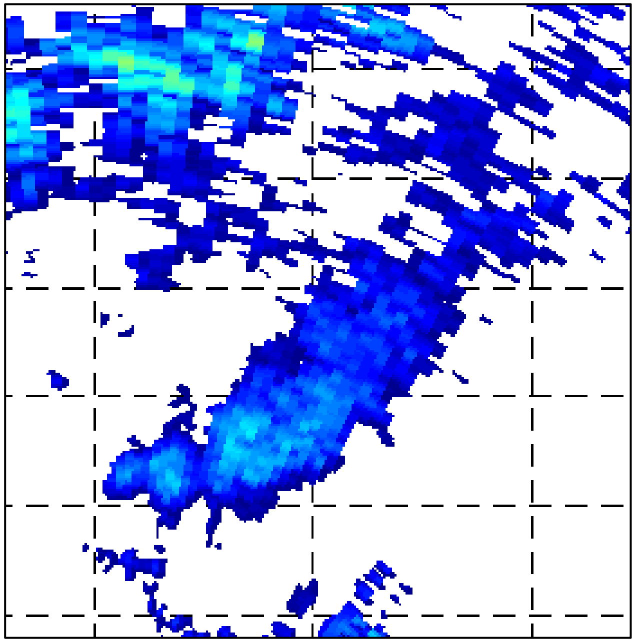

06:04:03 UTC
50m range resolution

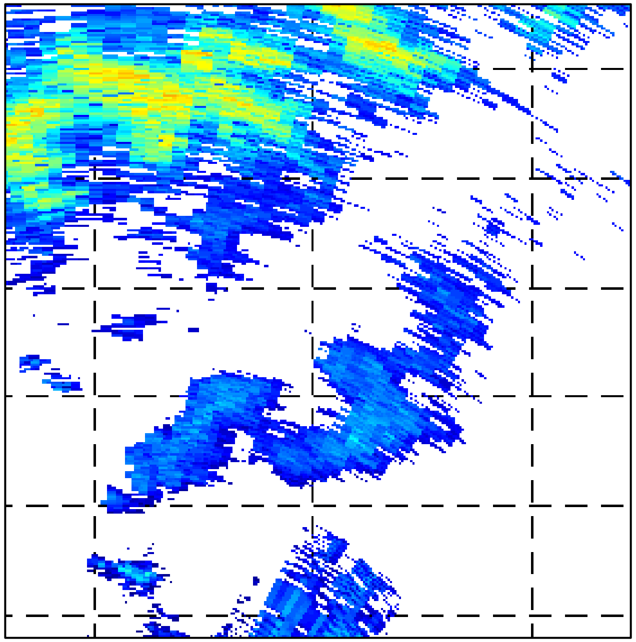

06:05:20 UTC
15m range resolution

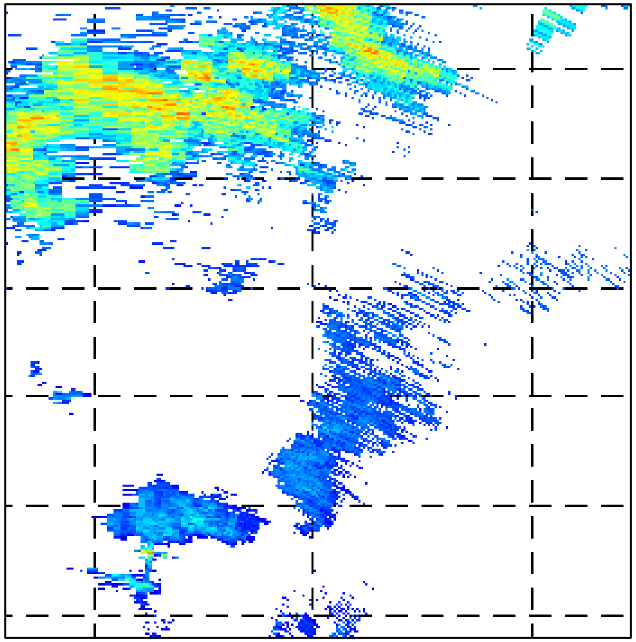

06:08:11 UTC
7m range resolution

Analysis

- Performed statistical analysis of collected polarimetric products from three observed bushfires
  - Two prescribed burns and one uncontrolled bushfire
  - Analyze differences between prescribed burns and uncontrolled bushfires
- Distributions of data collected are shown below
  - Mean and variation of Z_{DR} consistent across each burn from 1-2dB
  - Mean ρ_{hv} during prescribed burns (Barossa Valley and Cox Scrub) is higher than that compared to uncontrolled bushfire (Cherryville)
    - Attribute difference to increased intensity during uncontrolled bushfire

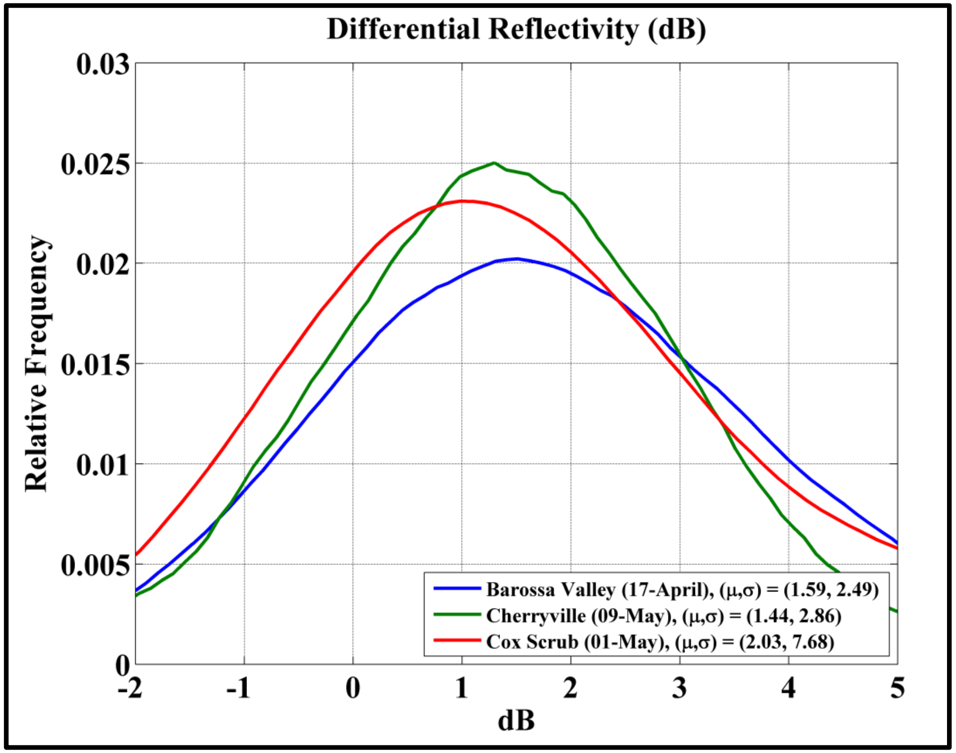

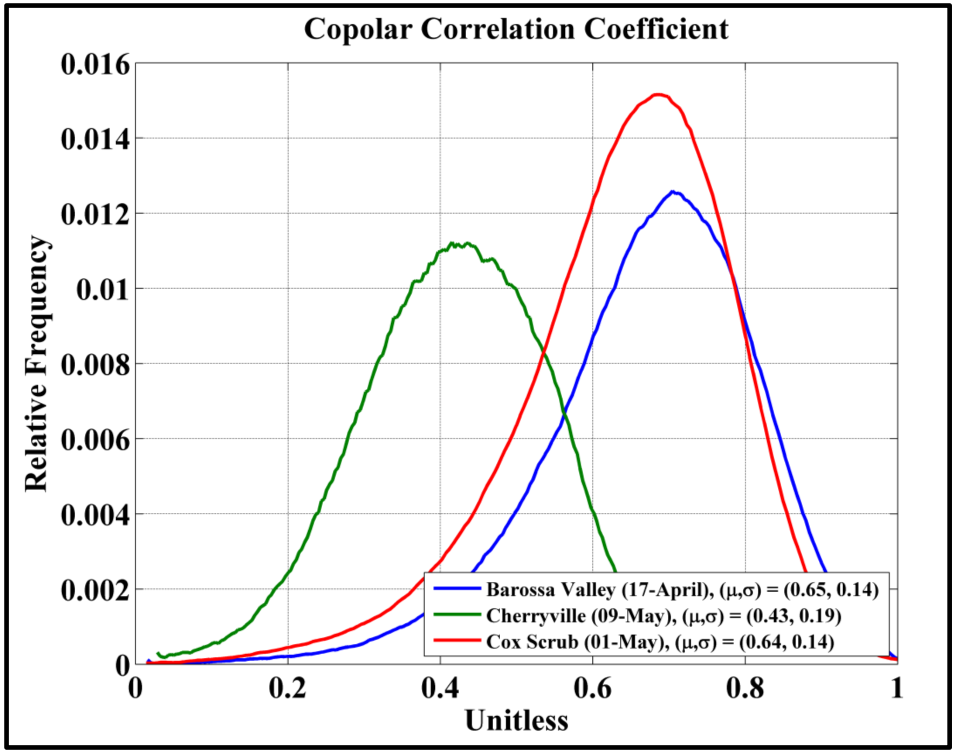

Observations

Prescribed Burn (17-April) - Weather

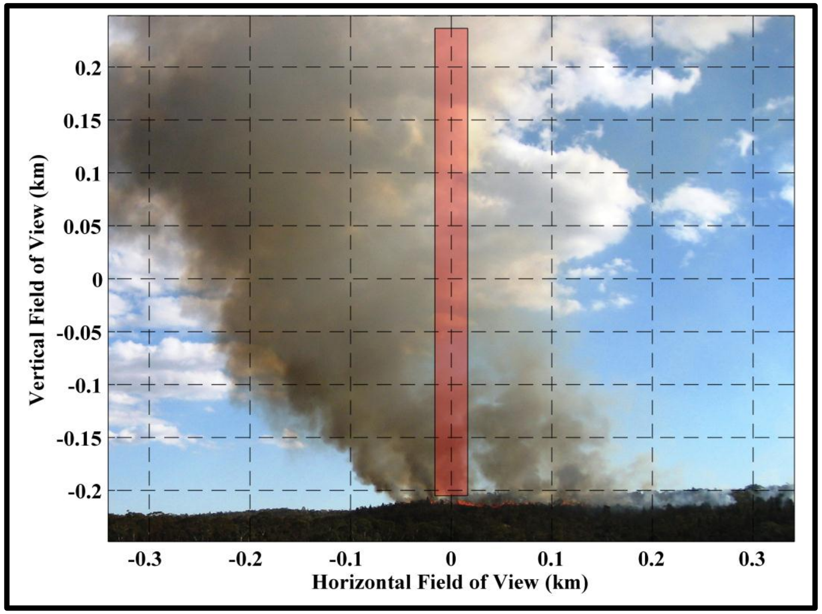

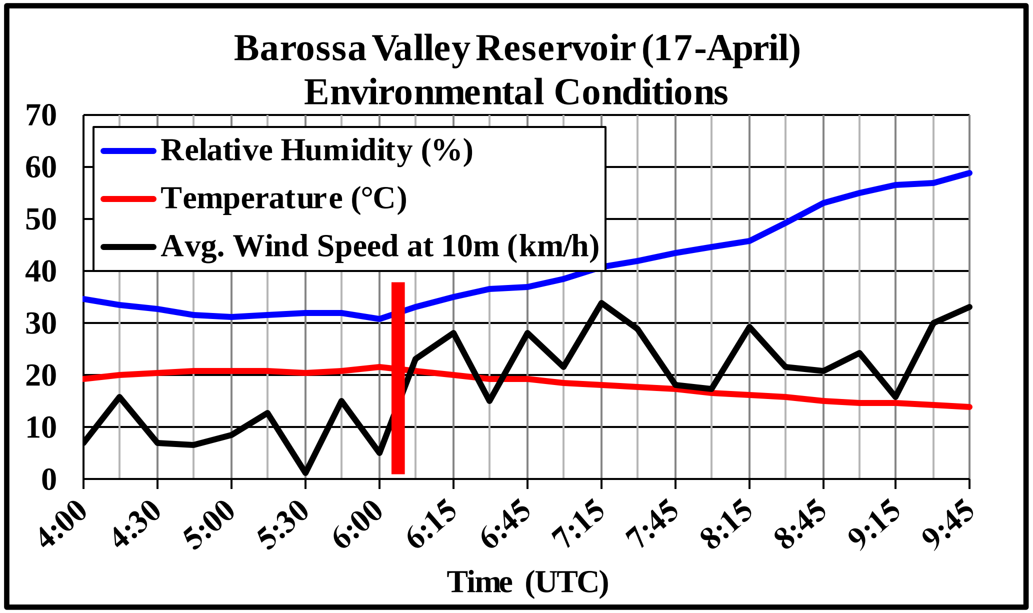

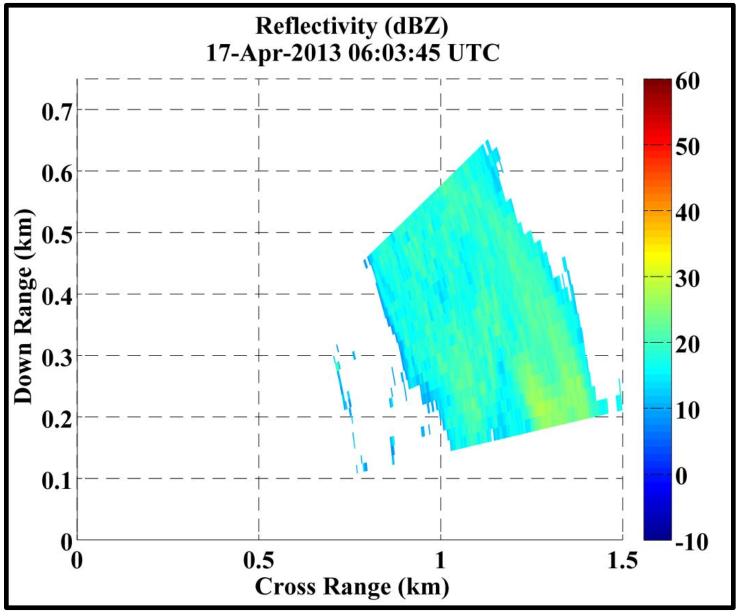

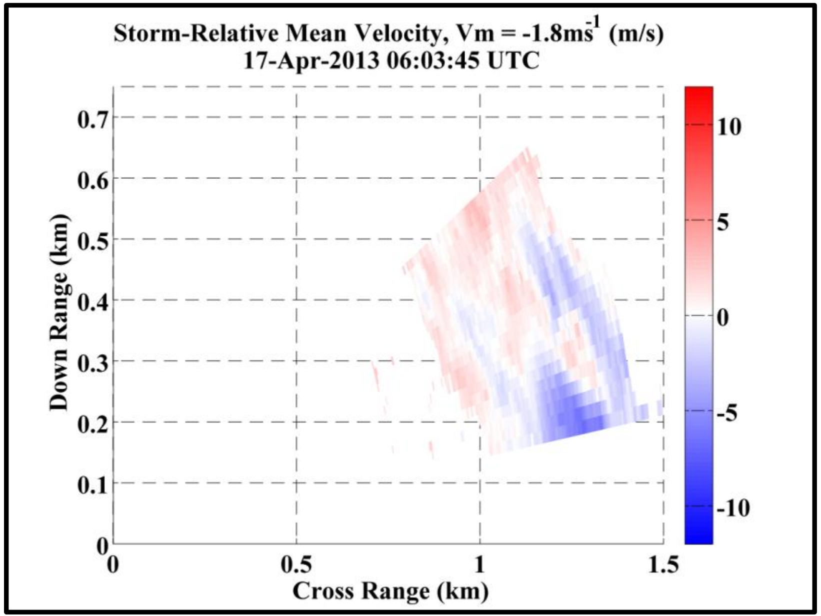

Observations

Uncontrolled Bushfire (10-May) - Weather

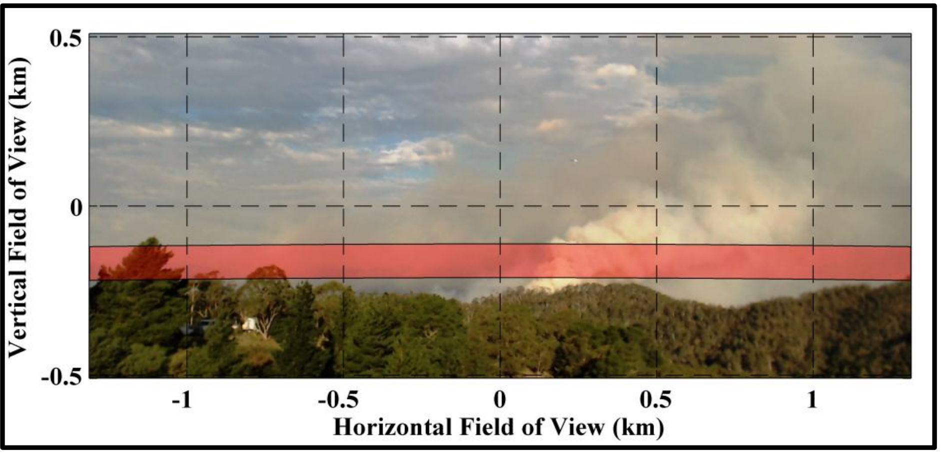

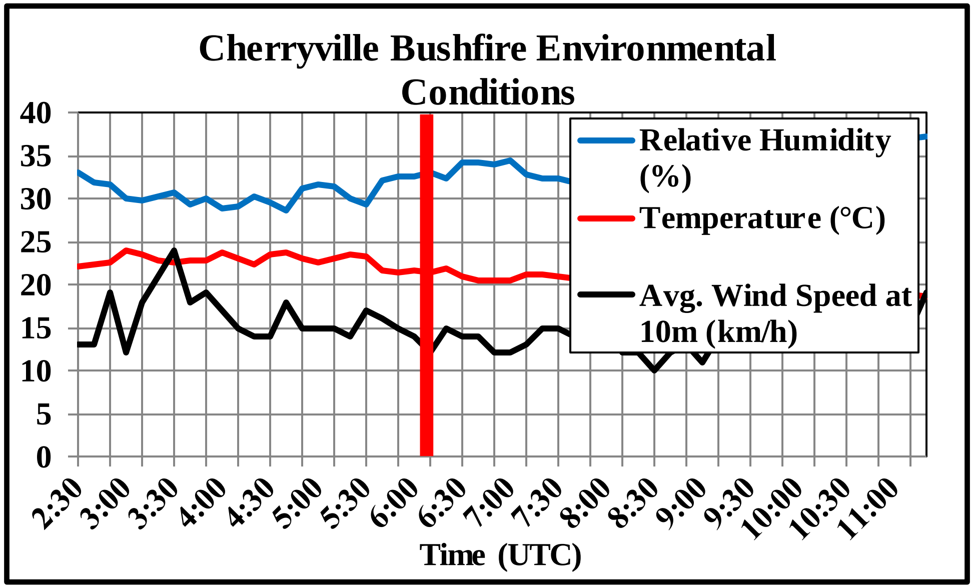

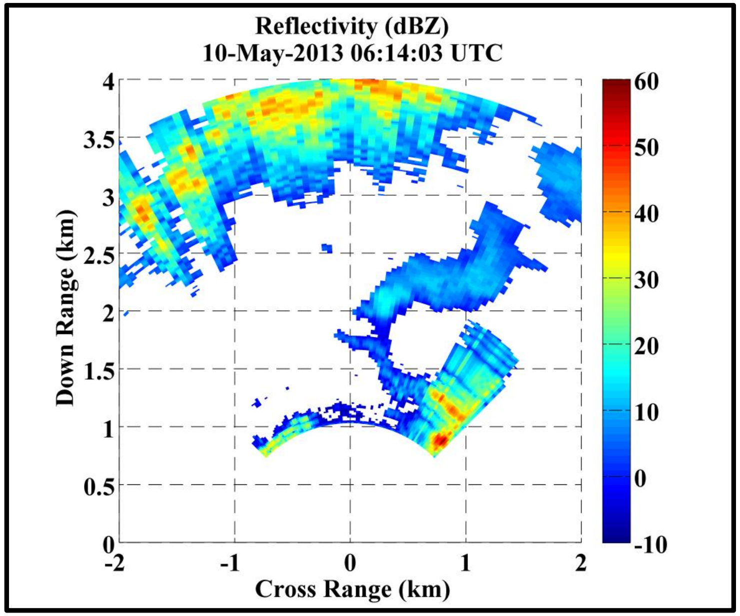

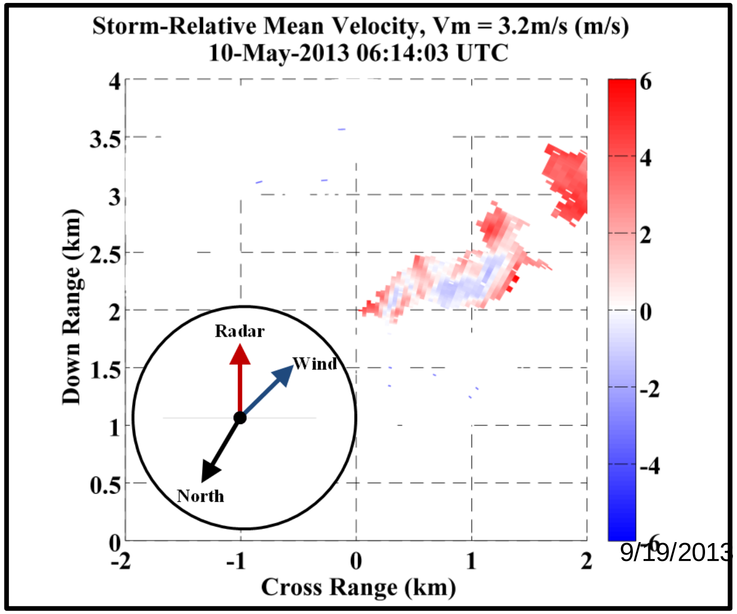

Observations

Uncontrolled Bushfire (10-May) - Weather